

Assessment of the Optic Nerve Disc and Excavation Parameters of Interactive and Automated Parameterization Methods

Dovilė BUTEIKIENĖ^{1,3}, Alvydas PAUNKSNIS¹,
Valerijus BARZDŽIUKAS³, Jolita BERNATAVIČIENĖ²,
Virginijus MARCINKEVIČIUS², Povilas TREIGYS²

¹*Eye Clinic, Hospital of Lithuanian University of Health Sciences Kaunas Clinics
Eivenių str. 2, Kaunas, Lithuania*

²*Vilnius University, Institute of Mathematics and Informatics
Akademijos str. 4, LT-08663 Vilnius, Lithuania*

³*Department of Ophthalmology, Neuroscience Institute, Lithuanian University of Health Sciences
Eiveniu str. 4, Kaunas, Lithuania*

*e-mail: {dovileb@me.com, alvydas@stratelus.com}, {jolita.bernataviciene,
virginijus.marcinkevicius, povilas.treigys}@mii.vu.lt*

Received: June 2011; accepted: August 2012

Abstract. Glaucoma is one of the most insidious eye diseases the occurrence and progression of which a human does not feel. This article provides a brief overview of the eye nerve parameterization methods and algorithms. Parameterization itself is an important task that provides and uniquely defines the structure of the optic nerve disc and further can be used in disease detection or other studies that require a parametric estimate of the eye fundus pattern. So far, planimetric completely automated parameterization of excavation from eye fundus images has not been investigated in detail in the scientific literature. In this article, the authors describe an automated excavation and parameterization algorithm and make the correlation analysis of parameters obtained by both automated and interactive techniques. The obtained results are then compared with those produced by Optical Coherence and Heidelberg Retina Tomography. Finally, the article discusses glaucoma disease detection abilities using the estimated parameters of the eye fundus structures, obtained by different parameterization techniques.

Keywords: automated excavation parameterization, comparison of parameterization techniques, parameter correlation analysis, glaucoma detection, automated eye fundus structure parameterization.

1. Introduction

The appearance of the optic nerve disc (OND) has been used to evaluate the glaucoma status since 1851, when Hermann von Helmholtz invented the ophthalmoscope and for the first time viewed the eye fundus in the living humans (Williams *et al.*, 2011). In the course of time, fundus examination methods have continued to improve (Sampaolesi *et al.*, 2009). Since 1887 the early fundus photography has progressed to today's digital

stereoscopic fundus images. In the period of 1950–1960 a monocular direct ophthalmoscope was presented (Pearce, 2009) and now it is used for modern eye fundus assessment in the inverse binocular ophthalmoscopy (Sampaolesi *et al.*, 2009).

But even the modern digital stereoscopic or inverse binocular ophthalmoscopic OND image is still assessed and interpreted subjectively. In daily work, the ophthalmologists must determine whether the OND appearance is normal or pathological and the decision is based only on their clinical practice (Bock *et al.*, 2010).

Glaucoma is a progressive optic neuropathy with intraocular pressure fluctuation, characteristic structural changes in OND reflected in the visual field (Spaeth *et al.*, 2006). Worldwide, apart from the cataract, it is the second leading cause of blindness (Nayak *et al.*, 2009), but the leading causes of irreversible blindness (O'Colmain *et al.*, 2011). Hence, early detection and prevention is the only way to avoid the total loss of vision.

Glaucoma diagnosis is based on the classic triad: elevated intraocular pressure, typical visual field defects, and structural changes in OND (John and Langley, 1995). But the effect of the intraocular pressure varies from patient to patient, hence, it is difficult to use standardized measurements for diagnosis (Guesalaga *et al.*, 2003) and OND damage precedes the visual field loss, to this end, recommended accurate and reproducible measurements of the disc are recommended (Jayasundera *et al.*, 2005).

The early and objective diagnosis of glaucoma is based on the OND and retinal nerve fiber structure assessment (Morgan *et al.*, 2005). Usually ophthalmologists estimate the quantitative parameters of the morphology of OND such as: OND, excavation (EXC) diameters, areas, neuroretinal rim (NRR) area and shape, and the ratios of OND, ECX, NRR parameters (Jegelevičius *et al.*, 2008).

Clinical decision-making is complicated by a large variation in OND size within a population as well as among populations (Hoffmann *et al.*, 2007), various combinations of OND glaucomatous damage and the inter- and intra-operator variability reported by many studies (Chrastek *et al.*, 2005).

Recently computer-assisted interactive planimetry algorithm has been created for more objective quantitative OND morphology description from the digital fundus photoplanimetric image (Correnti *et al.*, 2003). The observer with a computer mouse draws the disc and excavation margins on the monitor of the computer and the software automatically calculates the various OND parameters (Lamoureux *et al.*, 2006). The main disadvantage of this method is that it is highly subjective, time-consuming and has a broad inter-observer variability (Xu *et al.*, 2008). The same conclusion was drawn from the investigation where fifteen ophthalmologists had described the optic nerve disc and excavation on six images of the same eye fundus (Tiešis and Treigys, 2010).

In recent years, various semi-automated, laser methods that enable a rapid image acquisition and measurement of OND have emerged (Sanfilippo *et al.*, 2009). Newer technologies, such as the optical coherence tomography and confocal scanning laser ophthalmoscopy, have allowed for a more objective measurement of OND than interactive methods. However, even those methods require a user's intervention to manually define the border of OND (or adjust to the optical coherence tomography case) leaving some inter-observer variability (Neubauer *et al.*, 2006).

All the above-described technologies are an efforts of researchers to overcome the lack of standardization, the inherent subjectivity and intra- as well as interobserver variability while evaluating the OND deformation in glaucoma (Corona *et al.*, 2002).

An objective, standardized, and precise evaluation of the OND morphology is crucial in the early diagnosis and follow-up management of glaucoma, but it still remains a problem. The analysis of ophthalmological images is a broad and multi-disciplinary field that is most effectively progressive when teams of scientists, engineers, and clinicians combine their forces to develop new techniques (Harvey and Lakshminarayanan, 2010).

At the first stage of the project sponsored by Lithuania State Science and Studies Foundation research group (Paunksnis *et al.*, 2006) developed an interactive method for the optic nerve disc and excavation parameterization. A rapid progress of information technologies has created new opportunities to develop a fully automated, objective, standardized, precise and low-cost parameterization of OND digital images (Treigys *et al.*, 2008). Recently, the mentioned automated optic nerve disc parameterization, developed by was updated with the ability to parameterize the excavation. In this article the authors present the updated algorithm and analyse parameterization performance and compares of the parameter sets produced by the interactive, Heidelberg Retina Tomography (HRT), and optical coherence tomography (OCT) techniques.

To test the parameterization quality and glaucoma-norm classification, control groups of patients were selected. 40 glaucoma (40 eyes, 6 males and 34 females, age 64 ± 9.6 years) and 32 norm (32 eyes, 12 males and 20 females, age 58.8 ± 5.7 years) patients with normal biometric parameters of the eye participated in the study. All subjects underwent a full ophthalmological examination, optic nerve disc colour digital fundus image, OCT and HRT at the same visit.

2. Description of Data Sets for the Analysis

Suppose that an array of the parameters x_1, x_2, \dots, x_k characterises a disease (or the health state), therefore it is possible to form k -dimensional vectors $X = (x_1, x_2, \dots, x_k)$ that correspond to patients. Let a set of the analysed data consist of s objects: X^1, X^2, \dots, X^s , where $X^i = (x_1^i, x_2^i, \dots, x_k^i)$, $i = 1, \dots, s$. The goal of classification is to assign the vectors X^1, X^2, \dots, X^s to one of the classes C_1, C_2, \dots, C_d . If X^i belongs to the class C_j ($j = 1, \dots, d$), X^i is called as a positive example for the class C_j , in the opposite, X^i is called as a negative example.

In this investigation, the objects under consideration are fundi of eyes (Fig. 1). Usually ophthalmologists estimate the parameters of the morphology of the optic nerve disc, excavation and neuroretinal rim visually. Excavation is the normally occurring depression or pit in the centre of the optic nerve disc, also called a physiologic excavation or cup. Neuroretinal rim is the tissue between the outer edge of the excavation and the outer margin of the optic nerve disc. They estimate the following parameters: vertical and horizontal diameters of the optic nerve disc; the area of the optic nerve disc; vertical and horizontal diameters of the excavation; area of the excavation; the area of the neuroretinal rim; four optic nerve disc sectors of the neuroretinal rim; the ratio between vertical

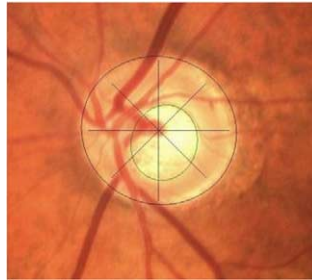


Fig. 1. Fundus of eye (the outer ellipse stands for the optic nerve disc approximation, inner for excavation approximation).

diameters of the EXC and OND; the ratio between horizontal diameters of the EXC and OND. Planimetry of the optic disc photographs allows us to estimate the morphologic parameters more precisely.

The analysed data set consists of multidimensional vectors X^i corresponding to the analysed fundi of eyes. 22 numerical parameters of the eye fundus have been measured. There are four groups of parameters (optic nerve disc, excavation (cup), neuroretinal rim, ratio between various parameters) presented in Table 1.

Table 1
Measured parameters of OND and EXC in the fundus image of the eye

No.	Full name of the parameter	Abbreviation
<i>Parameters of optic nerve disc (OND)</i>		
x_1	Horizontal diameter	<i>OND_HDiam</i>
x_2	Vertical diameter	<i>OND_VDiam</i>
x_3	Area	<i>OND_area</i>
x_4	Perimeter	<i>OND_P</i>
<i>Parameters of excavation (EXC)</i>		
x_5	Horizontal diameter	<i>EXC_HDiam</i>
x_6	Vertical diameter	<i>EXC_VDiam</i>
x_7	Area	<i>EXC_area</i>
x_8	Perimeter	<i>EXC_P</i>
<i>Ratios between various parameters</i>		
x_9	Ratio of EXC and OND horizontal diameters	<i>ratio_H</i>
x_{10}	Ratio of EXC and OND vertical diameters	<i>ratio_V</i>
<i>Parameters of neuroretinal rim (NRR)</i>		
x_{11}	Thickness of neuroretinal rim in the direction of 1 o'clock	<i>NRR-1</i>
x_{12}	Thickness of neuroretinal rim in the direction of 2 o'clock	<i>NRR-2</i>
...
x_{22}	Thickness of neuroretinal rim in the direction of 12 o'clock	<i>NRR-12</i>

Glaucoma is a group of diseases of the optic nerve involving the loss of retinal ganglion cells in a characteristic pattern of optic neuropathy (Nayak *et al.*, 2009). An increase in the physiological excavation is typical of glaucoma. However, this disease can be diagnosed even without the parameters of excavation, just basing on the tests (increase of intraocular pressure, glaucomatous visual field defects, analysis of the retinal nerve fibre layer). We analysed only the cases where an excavation was detected in the photographs.

3. Parameterization of Eye Fundus Anatomic Structures

All the ophthalmic images were parameterised by two algorithms. One of the algorithms was interactive and the other – fully automated. The eye fundus images were obtained at the Department of Ophthalmology, Institute of Neurosciences, Lithuanian University of Health Sciences, using the fundus camera Zeiss Visucam NM NM/FA 45° angle, positioning on the optic nerve disc with the resolution of 5 Mpixel images (image size 1958×2942). The common magnification quotient 0.5 and image diameter size is 7.4 mm. The scale (mm/pixels) for the fundus camera was 0.00503.

The first algorithm is a computer-assisted digital fundus images parameterization tool that implements the interactive optic nerve disc and excavation parameterization, when the demarcation line is drawn around the areas of interest with a computer mouse. The software was developed by Biomedical Engineering Institute of Kaunas University of Technology in the Matlab programming environment (The MathWorks Inc., 2007). Using software tools with a computer mouse on the digital fundus image an ophthalmologist points the approximate centre of the optic nerve disc, then, with the help of template, selects 12 points on the boundary of OND and excavation. The area of the disc was defined as the area within Elschning's ring, the excavation was defined on the basis of the contour, not pallor, the rim/excavation border was taken as the level at which the slope of the rim steepens. Then, the software approximates ellipses using the least squares algorithm on these points and calculates 22 numerical parameters (see Table 1) using the ellipses of the external optic nerve disc and excavation boundaries (Bourne *et al.*, 2009). The parameters used in this study were: optic nerve disc, excavation and rim areas, EXC/OND, and NRR/OND area ratios, vertical and horizontal EXC/OND diameter ratios.

The second algorithm, used for anatomical eye fundus structure parameterization, was completely automated. The algorithm for optic nerve disc parameterization in detail is described in the paper (Treigys *et al.*, 2008). However, since, in this paper, the approximation of excavation will be discussed and is dependent on the optic nerve disc approximation result, the main steps of optic nerve disc approximation will be recalled.

As it can be seen from Fig. 1, the blood vessels divide the area of the optic nerve disc into numerous non-homogenous regions. This effect is very undesirable and burdensome to optic nerve disc parameterization. Even more, since the excavation lies in the area of OND, the elimination of blood vessels in the eye fundus images is crucial. The authors have shown that blood vessels from the area of OND can be precisely removed by closing operation of mathematical morphology. Also, it has been estimated by experiments that a

disc-shaped structuring element with the diameter of 14 pixels is enough in order to efficiently remove the vasculature from OND. However, if such a diameter element performs well on blood vessel removal and preserves the size and boundary of the optic nerve disc, then it has a negative impact on the excavation structure. The size of excavation may be of order of the blood vessel size and such a structuring element just eliminates the excavation by removing edge gradient information. Thus, the size of the structuring element should be properly selected in order to detect the excavation. For the proper diameter selection as well as for other parameters, discussed later in this paper, a discrete Bayes optimization method will be introduced.

Further, with a view to find the boundaries of the optic nerve disc, the authors introduced a Canny edge detection algorithm. This algorithm depends on two parameters: low and high threshold levels τ_1 and τ_2 . The authors used the Otsu clusterization method to calculate those parameters. However, calculated parameters are scaled because of the presence of noise after the application of the morphological closing operation. These two parameters are of utmost importance, since if they are wrongly selected, the boundary of an object will not be found or it could become discontinuous and further may be treated as noise. Next, an approximate optic nerve disc position is found by applying the iterative circular Hough transform. Finally, the elliptical parameters describing OND were found by the least squares method. The least squares algorithm calculates minor and major axes, inclination angle and centre coordinates of an ellipse.

3.1. Approximation of Excavation

Firstly, the area containing an excavation must be cropped from the eye fundus image. The cropping is very important, since the pixels intensity change of excavation and optic nerve disc itself in most cases does not introduce high gradient values. Thus, if a lower pixel intensity values, representing retina together with optic nerve disc and excavation pixel intensities, were fetched to the threshold selection method, then the information on the excavation boundary will be lost. This would happen because the gradient between the retina and optic nerve disc changes more rapidly. On the other hand, then the excavation with respect to other eye fundus structures is quite small, if the location of excavation is not precise enough, the boundary of a structure may be interpreted as a noise or some blood vessel formation. Hence, with a view to specify the region of interest (ROI), we use the major axis of the optic nerve disc ellipse found by an automated algorithm. The centre of ROI becomes the ellipse centre. This region of interest then is cropped from the green channel of the initial eye fundus image. Next, a constrained Bayes method, described in Section 4 is initialized for discrete parameter estimation. The Bayes algorithm is set to 300 times to estimate three different parameter values. The parameters to be optimized are the structuring element diameter and two Canny algorithm threshold levels. These three parameters are constrained. The threshold levels are constrained by the maximum pixel intensity level and the structuring element diameter by a minor axis. Then, with the set of parameters proposed by the Bayes method, the region of interest area is processed, as described in Section 3, i.e., the algorithm computes the morphological closing,

Canny edge detection, iterative Hough transform, and elliptical least squares fitting to the gathered excavation boundary points.

Next, the error of elliptical approximation and the circle-shape preservation is estimated and consequently, the result is returned back to the Bayes optimization algorithm to calculate the new estimates of diameter and two threshold levels. The error measurement function was calculated as follows:

$$\frac{\sum_{i=1}^N \left(\frac{(x_c - x_i)^2}{a^2} + \frac{(y_c - y_i)^2}{b^2} - 1 \right)^2 P^2}{4NS\pi}. \quad (1)$$

Here x_c and y_c coordinates define the centre of ellipsis; x_i and y_i are boundary point coordinates that describe the excavation; P and S are a perimeter and an area, respectively, of a convex hull defined by the boundary points; N is the number of boundary points.

In such a way the procedure is repeated 300 times. The minimum value of the error function denotes the best elliptical approximation of the excavation within the area of the optic nerve disc.

4. Classification Methods

In this investigation, the system ‘‘Orange’’ (Demsar *et al.*, 2004) is used for experiments. Classification methods were used: Naïve Bayes (John and Langley, 1995), classification trees (Breiman *et al.*, 1984), support vector machine and the kNN classifiers (Dunham, 2003), and C4.5 (Quinlan, 1993).

The Naïve Bayes classifier (John and Langley, 1995) is based on the Bayes probability rule and the two assumptions: parameters are relatively independent of one another and, second, there are no hidden or invisible parameters that influence the process of class assignment.

Suppose that each record X_i of the training data set consists of j independent discrete parameters $x_{i1}, x_{i2}, \dots, x_{ij}$. Then the probability that the observed record of discrete parameters X_i belongs to class C_l , is calculated by the formula:

$$P(C_l|X_i) = \frac{P(C_l) \cdot P(X_i|C_l)}{P(X_i)}. \quad (2)$$

An a priori probability of the class appearance $P(C_l)$ is calculated from the training set. Based on the assumption that the parameters are independent of one another and by using the data from the training set, we can calculate a conditional probability $P(X_i|C_l) = \prod_{j=1}^n P(x_{ij}|C_l)$. Moreover, in (2), the probability provided in the denominator does not depend on the class. This fact means that it does not influence the maximum likelihood solution (3). Such a scheme guarantees that every record X_i is assigned to the class that has the highest conditional probability.

$$C = \operatorname{argmax}_{C_l} P(C_l|X_i) = \operatorname{argmax}_{C_l} P(C_l) \cdot P(X_i|C_l). \quad (3)$$

If the training records incorporate the continuous parameters, then an assumption is made that, for each class C_l , those continuous parameters are distributed according to the normal Gaussian distribution $\Phi_l(x_{ij}) = N(x_{ij}, \mu_{lj}, \sigma_{lj})$. Here parameters μ_{lj} and σ_{lj} are calculated on the training set of the l th class for the j th parameter. Then the conditional probability can be expressed as $P(X_i|C_l) = \prod_{j=1}^n \Phi_l(x_{ij})$. However, this transition is not always correct. In such cases, continuous parameters are forced to take a discrete form. The main advantage of the Naïve Bayes classifier is that it is simple and fast, and, in most cases, if the parameters are independent from one another, the classification accuracy is satisfactory. In other cases, this classifier gives poor results (Liu, 2006).

Using a classification tree technique, a tree is constructed to model the classification process. Classification tree methods are a good choice when the data mining task is the classification or prediction of outcomes and the goal is to generate rules that can be easily understood and explained. Once the tree has been formed, it is applied to each item in the data set and results in the classification for that item. Classification tree describes a structure wherein the leaves represent classifications and branches represent conjunctions of features that lead to those classifications. A classification tree can be learned by splitting the source set into subsets, based on an attribute value test. This process is repeated on each derived subset in a recursive manner. The recursion is completed when splitting is either non-feasible, or a singular classification can be applied to each element of the derived subset (Breiman *et al.*, 1984). C4.5 is an algorithm used to generate a decision tree developed by Ross Quinlan (1993). It was used to classification tree construction. This algorithm handles both, a discrete and a continuous value, prunes the tree after creation, and is able to handle the attributes with different costs.

The k nearest neighbours (kNN) technique assumes that the entire training set includes not only the data in the set, but also the desired classification for each item. The training data become a model. When a classification is to be made for a new item, its distance, usually Euclidian, to each item in the training set must be determined. Only the k closest entries in the training set are considered further. The new item is then placed in the class that contains most items from this set of the k closest items. The kNN technique is extremely sensitive to the value of k (Dunham, 2003).

The support vector machine classifier (SVM) is the classification method that executes the classifier training steps and may be used in the regression analysis tasks as well. When the SVM method is applied to the classification task, the method creates a hyper-plane that allows attributing the data points to two classes (Cristiani and Shawe-Taylor, 2003). Assuming that the training set is comprised of X_i objects and each of these objects corresponds to the class C_l , then the initial data are paired as (X_i, C_l) , $i = 1, \dots, m$. Here m represents the count of training set objects, $X_i \in \mathbb{R}^n$ and $C_l = \{-1, 1\}$. Afterwards, the simplest support vector machine classifier creates a hyper-plane according to the equation $(W \cdot X^T) + b = 0$, $W \in \mathbb{R}^n$, $b \in \mathbb{R}$ that corresponds to the objective function $f(x) = \text{sign}((W \cdot X^T) + b)$. Here $W = (w_1, w_2, \dots, w_n)$ as well as $X = (x_1, x_2, \dots, x_n)$ are row vectors, and $W \cdot X^T = \sum_{i=1}^n w_i x_i$ is a product of row vectors.

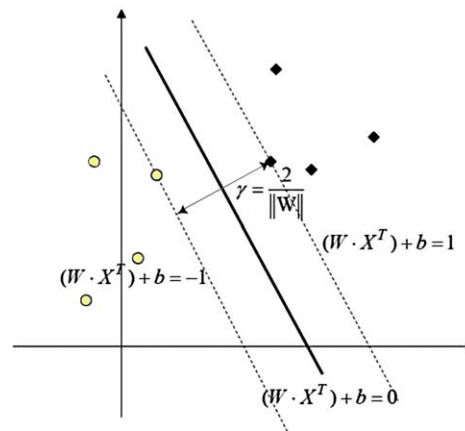


Fig. 2. Scheme of support vector machine classifier.

After the hyper plane has been created, the training set objects are divided into two classes such that the distance between the closest elements, belonging to different classes, and the hyper-plane boundary is maximal (Bernataviciene, 2008). Figure 2 shows the class separation by the SVM.

Figure 2 illustrates the hyper-plane that is marked as straight line and samples of two classes. Rounded and diamond samples belongs to different classes. It is worthwhile noticing that the created hyper-plane is appertained to the subset of the training set that consists of the so-called support vectors. To represent the hyper-plane in a suitable way, the proposed algorithm calculates $\min_{W,b} \frac{1}{2} \|W\|^2$ with respect to $C_i((W \cdot X_i^T) + b) \geq 1, i = 1, \dots, m$. Then, the maximum distance between different class boundaries is $\gamma = \frac{2}{\|W\|}$. The issues related to the support vector machine method application to visualize data are discussed in the paper (Kurasova, 2009).

5. Results of a Parameter Correlation Analysis

As already mentioned, the testing set consists of 72 fundus images that were parameterized by the automated and interactive algorithms. Besides the standard eye fundus examining technique, during which a planar photograph of the eye fundus was taken, all the investigative persons were additionally examined by the Optical Coherence Tomography and Heidelberg Retina Tomography. It is important to note that the tomography investigation results are formed according to the 3D laser scan of an object, i.e., optic nerve disc, excavation, and neuroretinal rim measurements are calculated according to stereometric parameters from the 3D laser scan. This technique substantially differs from the planimetric eye fundus image analysis and object parameterization by interactive and automated algorithms, since it does not give the object's depth evaluation. Moreover, these techniques are measuring a different set of eye fundus parameters. Thus, further this section will be organized as follows: in the first part of this section, a correlation

Table 2
Correlation of OCT and HRT parameters (all cases)

	<i>OCT</i> (<i>OND_area</i>)	<i>OCT</i> (<i>EXC_area</i>)	<i>OCT</i> (<i>ratio_V</i>)	<i>OCT</i> (<i>ratio_H</i>)	<i>OCT (EXC_area/</i> <i>OND_area ratio)</i>
<i>HRT (OND_area)</i>	0.718	0.548	0.312	0.289	0.335
<i>HRT (EXC_area)</i>	0.656	0.829	0.669	0.716	0.752
<i>HRT (ratio_V)</i>	0.422	0.522	0.398	0.602	0.526
<i>HRT (ratio_H)</i>	0.566	0.772	0.748	0.743	0.790
<i>HRT (EXC_area/</i> <i>OND_area ratio)</i>	0.446	0.718	0.672	0.752	0.761

Table 3
Correlation of OCT and HRT parameters (glaucoma case)

	<i>OCT</i> (<i>OND_area</i>)	<i>OCT</i> (<i>EXC_area</i>)	<i>OCT</i> (<i>ratio_V</i>)	<i>OCT</i> (<i>ratio_H</i>)	<i>OCT (EXC_area/</i> <i>OND_area ratio)</i>
<i>HRT (OND_area)</i>	0.726	0.581	0.306	0.258	0.333
<i>HRT (EXC_area)</i>	0.647	0.803	0.652	0.694	0.721
<i>HRT (ratio_V)</i>	0.484	0.691	0.625	0.781	0.740
<i>HRT (ratio_H)</i>	0.510	0.748	0.789	0.801	0.809
<i>HRT (EXC_area/</i> <i>OND_area ratio)</i>	0.385	0.646	0.629	0.729	0.711

Table 4
Correlation of OCT and HRT parameters (normal case)

	<i>OCT</i> (<i>OND_area</i>)	<i>OCT</i> (<i>EXC_area</i>)	<i>OCT</i> (<i>ratio_V</i>)	<i>OCT</i> (<i>ratio_H</i>)	<i>OCT (EXC_area/</i> <i>OND_area ratio)</i>
<i>HRT (OND_area)</i>	0.705	0.516	0.357	0.364	0.367
<i>HRT (EXC_area)</i>	0.675	0.807	0.517	0.735	0.701
<i>HRT (ratio_V)</i>	0.392	0.424	0.168	0.470	0.353
<i>HRT (ratio_H)</i>	0.654	0.702	0.477	0.496	0.572
<i>HRT (EXC_area/</i> <i>OND_area ratio)</i>	0.536	0.779	0.521	0.756	0.720

analysis between planimetric and stereometric parameters will be provided; in the second part, the classification results according to the parameters from planimetric algorithms that describe the optic nerve disc, excavation, and neuroretinal rim will be discussed.

The results provided in Tables 2, 3, and 4 shows a correlation between the parameters of the optic nerve disc and excavation that were measured by OCT and HRT scans of the same eye of an investigative person.

The results provided in Tables 2, 3, and 4 show that, despite the new technological achievements and different device implementations that are capable to perform a laser scan of a human eye fundus and to calculate the optic nerve disc and excavation parameters, there is rather a strong correlation between the measured parameters by different techniques. Weak correlation is between *ratio_V* parameters of different techniques in norm case. This fact implies that even if the newest technological achievements are used for the human examination, the task of eye fundus structures evaluation is extremely difficult and leads to different results. Moreover, tomograph scan result shows that the correlation between anatomical structure parameters of different tomography means, used for eye fundus scanning, is neither better nor worse no matter there is a disease or not, except the parameter *ratio_V* and *ratio_H*.

For the second part of the correlation analysis, an ophthalmologist has visually inspected the optic nerve disc and excavation approximation results obtained by the automated algorithm. It was concluded that there were 9 wrong parameterization cases of OND structure and 16 wrong parameterization cases of EXC structure respectively out of 72 eye fundus images.

Further, Tables 5, 6, and 7 show the parameter correlation results in case the parameters are calculated from planimetric eye fundus images by the interactive and automated algorithms for eye fundus anatomical structures parameterization. Besides, the same persons the same eye images were parameterized.

The results shown in Tables 5, 6, and 7 indicate that the optic nerve disc parameters as well as the excavation parameters, calculated by the interactive and automated algorithms do have a strong correlate. In most cases, the correlation is similar to that presented in Tables 2, 3, and 4. The correlation between the parameters that are gathered by means of tomography and image analysis was not calculated, since the image analysis algorithms are evaluating the parameters of the optic nerve head and excavation without any depth information about the anatomical structure. Moreover, the interactive algorithm is as much interactive as it calculates an elliptical cone by the least squares from 12 points that were put on the eye fundus image by an ophthalmologist with a view to describe the optic nerve disc as well as excavation. Regarding this fact a conclusion on planimetric

Table 5
Correlation of interactive and automated algorithm results (all cases)

	<i>Interact</i> (<i>OND_area</i>)	<i>Interact</i> (<i>EXC_area</i>)	<i>Interact</i> (<i>ratio_V</i>)	<i>Interact</i> (<i>ratio_H</i>)	<i>Interact</i> (<i>EXC_area/</i> <i>OND_area ratio</i>)
<i>Auto (OND_area)</i>	0.583	0.470	0.275	0.261	0.287
<i>Auto (EXC_area)</i>	0.610	0.813	0.651	0.660	0.716
<i>Auto (ratio_V)</i>	0.396	0.689	0.629	0.648	0.683
<i>Auto (ratio_H)</i>	0.372	0.629	0.554	0.616	0.624
<i>Auto (EXC_area/</i> <i>OND_area ratio)</i>	0.422	0.746	0.673	0.691	0.743

Table 6
Correlation of interactive and automated algorithm results (glaucoma case)

	<i>Interact</i> (<i>OND_area</i>)	<i>Interact</i> (<i>EXC_area</i>)	<i>Interact</i> (<i>ratio_V</i>)	<i>Interact</i> (<i>ratio_H</i>)	<i>Interact</i> (<i>EXC_area/</i> <i>OND_area ratio</i>)
<i>Auto (OND_area)</i>	0.539	0.528	0.353	0.327	0.355
<i>Auto (EXC_area)</i>	0.659	0.796	0.586	0.593	0.638
<i>Auto (ratio_V)</i>	0.433	0.658	0.521	0.549	0.584
<i>Auto (ratio_H)</i>	0.391	0.605	0.493	0.549	0.561
<i>Auto (EXC_area/</i> <i>OND_area ratio)</i>	0.478	0.712	0.585	0.609	0.650

Table 7
Correlation of interactive and automated algorithm results (normal case)

	<i>Interact</i> (<i>OND_area</i>)	<i>Interact</i> (<i>EXC_area</i>)	<i>Interact</i> (<i>ratio_V</i>)	<i>Interact</i> (<i>ratio_H</i>)	<i>Interact</i> (<i>EXC_area/</i> <i>OND_area ratio</i>)
<i>Auto (OND_area)</i>	0.676	0.317	0.062	0.119	0.101
<i>Auto (EXC_area)</i>	0.465	0.788	0.634	0.685	0.755
<i>Auto (ratio_V)</i>	0.330	0.701	0.619	0.663	0.706
<i>Auto (ratio_H)</i>	0.308	0.637	0.548	0.621	0.640
<i>Auto (EXC_area/</i> <i>OND_area ratio)</i>	0.276	0.755	0.691	0.713	0.798

and stereometric eye fundus structure parameterization technique can be drawn. That is, in the stereometric case, the correlation between parameters shows that, regardless of the technique used for eye fundus examination, the interpretation of structures is quite different, since the parameter estimates do not match even if the depth of the structure is known. In the planimetric case, the parameter correlation analysis shows the same result. However, if we think about the correlation result in respect of the automated and interactive optic nerve disc and excavation parameter estimation, then the parameter correlation analysis proves that the automated algorithm recognizes and parameterizes eye fundus structures in a similar manner as the ophthalmologist does.

The third part of the optic nerve disc and excavation parameters analysis covered the classification task. The parameters collected by different means, i.e., interactive algorithm, automated algorithm, OCT, and HRT, were introduced to four classifiers that are freely available in the open source packet Orange (Curk *et al.*, 2005). At the beginning, all the 22 parameters were fed to the classifiers. The cross-validation learning rule was tested on 10 folds. Table 7 presents the classification results by the interactive algorithm data and Table 8 the classification of the automated algorithm data. Table 9 presents the confusion matrices produced by the best classifiers. In addition, a linear classifier was

Table 8
Classification results of all the 22 parameters found by interactive algorithm

	<i>Classifier accuracy</i>	<i>Sensitivity</i>	<i>Specificity</i>	<i>Area under curve</i>
<i>C4.5</i>	0.5607	0.3750	0.7812	0.5979
<i>kNN</i>	0.5857	0.6750	0.4688	0.6104
<i>SVM</i>	0.7250	0.7500	0.6875	0.7708
<i>Naïve Bayes</i>	0.6839	0.6750	0.6875	0.7542
<i>Classification Tree</i>	0.5732	0.6000	0.5312	0.5906

Table 9
Classification results of all the 22 parameters found by automated algorithm

	<i>Classifier accuracy</i>	<i>Sensitivity</i>	<i>Specificity</i>	<i>Area under curve</i>
<i>C4.5</i>	0.6089	0.7250	0.4688	0.6156
<i>kNN</i>	0.5982	0.6500	0.5313	0.6385
<i>SVM</i>	0.5821	0.8500	0.2500	0.5708
<i>Naïve Bayes</i>	0.6661	0.6500	0.6875	0.7271
<i>Classification Tree</i>	0.5161	0.5500	0.4688	0.5156

Table 10
Confusion matrices obtained by SVM and Naïve Bayes classifiers

	<i>Interactive algorithm</i>			<i>Automated algorithm</i>		
	<i>Glaucoma</i>	<i>Normal</i>		<i>Glaucoma</i>	<i>Normal</i>	
<i>Glaucoma</i>	26	14	40	26	14	40
<i>Normal</i>	11	21	32	15	17	32
<i>Count</i>	37	35	72	41	31	72

used in support vector machine algorithm. Here and further in the article bold values denotes the best classifier.

As it can be seen from Tables 8 and 9 the classification accuracy is better when the parameters computed by the interactive algorithm were used. Besides, confusion matrices presented in Table 10, confirm that a correct class assignment is better with the parameters produced by the interactive algorithm for the normal case. However, the glaucoma class identification remains the same with the parameters produced by both methods.

For the second experiment, parameters that described the neuroretinal rim were excluded. The experiment was accomplished only with the first ten parameters that describe the optic nerve disc and excavation. The same cross validation conditions, as mentioned above, were applied.

The results presented in Tables 11, 12, and 13 imply the same conclusion, that the classifier accuracy is better when the parameters found by the interactive algorithm were

Table 11
Classification results of the first 10 parameters found by interactive algorithm

	<i>Classifier accuracy</i>	<i>Sensitivity</i>	<i>Specificity</i>	<i>Area under curve</i>
<i>C4.5</i>	0.6429	0.5500	0.7500	0.6708
<i>kNN</i>	0.5571	0.6000	0.5000	0.5813
<i>SVM</i>	0.7411	0.7750	0.6875	0.7646
<i>Naive Bayes</i>	0.6714	0.6500	0.6875	0.6792
<i>Classification Tree</i>	0.6143	0.5750	0.6562	0.6188

Table 12
Classification results of the first 10 parameters found by automated algorithm

	<i>Classifier accuracy</i>	<i>Sensitivity</i>	<i>Specificity</i>	<i>Area under curve</i>
<i>C4.5</i>	0.5679	0.7750	0.3125	0.5406
<i>kNN</i>	0.6018	0.6500	0.5313	0.7083
<i>SVM</i>	0.6804	0.8500	0.4688	0.7354
<i>Naive Bayes</i>	0.6268	0.7000	0.5313	0.6104
<i>Classification Tree</i>	0.5696	0.6500	0.4688	0.5687

Table 13
Confusion matrices obtained by the SVM classifier

	<i>Interactive algorithm</i>			<i>Automated algorithm</i>		
	<i>Glaucoma</i>	<i>Norma</i>		<i>Glaucoma</i>	<i>Normal</i>	
<i>Glaucoma</i>	28	12	40	30	10	40
<i>Normal</i>	9	23	32	10	22	32
<i>Count</i>	37	35	72	40	32	72

used for classification. However, the parameters obtained by the automated algorithm suit better for glaucoma detection, since 30 correct glaucoma cases were identified from 40, while the parameters from the interactive algorithm were able to describe 28 glaucoma cases out of the same 40 cases.

Further, the parameters produced by stereometric eye fundus structure parameterization techniques, were analysed and the classification performance was investigated as well. However, the parameters set produced by Heidelberg retina and Optical Coherence Tomographs are not quite coincident. Moreover, these parameter sets also are not coincident with ones obtained by the automated and interactive methods as well. Thus, with a view to check the classification results of parameters that were obtained by the stereometric eye fundus structure parameterization technique, a set of coincident parameters was calculated. Parameters that were fed to the classifiers were: optic nerve disk area, excavation area, the ratio of vertical optic nerve disc and excavation, the ratio of hori-

Table 14
Classification results of five derived parameters found by the interactive algorithm

	<i>Classifier accuracy</i>	<i>Sensitivity</i>	<i>Specificity</i>	<i>Area under curve</i>
<i>C4.5</i>	0.6018	0.5250	0.6875	0.6844
<i>kNN</i>	0.7214	0.7250	0.7188	0.7875
<i>SVM</i>	0.7482	0.8000	0.6875	0.7604
<i>Naïve Bayes</i>	0.6768	0.7000	0.6562	0.7188
<i>Classification Tree</i>	0.7393	0.8000	0.6562	0.7615

Table 15
Classification results of five derived parameters found by the automated algorithm

	<i>Classifier accuracy</i>	<i>Sensitivity</i>	<i>Specificity</i>	<i>Area under curve</i>
<i>C4.5</i>	0.6661	0.9500	0.3125	0.5958
<i>kNN</i>	0.4679	0.5250	0.4062	0.5625
<i>SVM</i>	0.6429	0.8250	0.4062	0.6063
<i>Naïve Bayes</i>	0.6518	0.8250	0.4375	0.6667
<i>Classification Tree</i>	0.5839	0.6250	0.5312	0.5906

Table 16
Confusion matrices obtained by the SVM and C4.5 classifiers, respectively

	<i>Interactive algorithm</i>			<i>Automated algorithm</i>		
	<i>Glaucoma</i>	<i>Normal</i>		<i>Glaucoma</i>	<i>Normal</i>	
<i>Glaucoma</i>	28	12	40	38	2	40
<i>Normal</i>	11	21	32	10	22	32
<i>Count</i>	39	33	72	48	24	72

zonal optic nerve disc and excavation, and the ratio of excavation-optic nerve disc area ratio. Tables 14 and 15 illustrate the classification results of five parameters obtained by the interactive and automated algorithms, respectively. Table 16 shows the best classifier confusion matrices. The same cross-validation conditions were applied as mentioned above.

Tables 17 and 18 illustrate the classification results of the five parameters obtained by the HRT and OCT tomographs, respectively. Table 18 shows the best classifier confusion matrices.

The results provided in Tables 14 and 15 indicate that the classification accuracy of the parameters, obtained by the interactive algorithm, outperforms the classification accuracy when used the parameter set found by automated algorithm. However, the same trend, as presented in Table 13 is seen. Table 16 shows that the parameters found by the automated algorithm suit better for glaucoma detection, since 38 correct glaucoma cases

Table 17
Classification results of five derived parameters obtained by HRT

	<i>Classifier accuracy</i>	<i>Sensitivity</i>	<i>Specificity</i>	<i>Area under curve</i>
<i>C4.5</i>	0.7500	0.7500	0.7500	0.7417
<i>kNN</i>	0.7482	0.8000	0.6875	0.7896
<i>SVM</i>	0.7250	0.8000	0.6250	0.7937
<i>Naïve Bayes</i>	0.7607	0.7500	0.7812	0.7875
<i>Classification Tree</i>	0.6786	0.8000	0.5312	0.7208

Table 18
Classification results of five derived parameters obtained by OCT

	<i>Classifier accuracy</i>	<i>Sensitivity</i>	<i>Specificity</i>	<i>Area under curve</i>
<i>C4.5</i>	0.6339	0.3750	0.9688	0.6708
<i>kNN</i>	0.5946	0.7000	0.4688	0.6833
<i>SVM</i>	0.6125	0.7250	0.4688	0.7208
<i>Naïve Bayes</i>	0.6375	0.5250	0.7812	0.7271
<i>Classification Tree</i>	0.5911	0.6500	0.5312	0.5312

Table 19
Confusion matrices obtained Naïve Bayes classifiers respectively

	<i>HRT</i>			<i>OCT</i>		
	<i>Glaucoma</i>	<i>Norma</i>		<i>Glaucoma</i>	<i>Norma</i>	
<i>Glaucoma</i>	30	10	40	21	19	40
<i>Norma</i>	8	24	32	7	25	32
<i>Count</i>	38	34	72	28	44	72

were identified from 40, while the parameters from the interactive algorithm were able to describe only 28 glaucoma cases out of the same 40 cases.

Further, in Tables 17 and 18, the glaucoma-norm classification results obtained by tomography techniques are presented. It can be seen, that the parameters produced by the Heidelberg Retina tomograph better describe the glaucoma when compared to those produced by Optical Coherence tomograph. The results obtained from HRT parameters are quite similar to those obtained by the interactive algorithm. Figure 3 shows the classification tree of the Heidelberg Retina tomograph parameters.

Figure 3 shows that with the view to gather more information about glaucoma prediction there are four most significant parameters produced by HRT. That is ratio of EXC area and OND area, ratio of EXC and OND vertical and horizontal diameters and EXC area as well. According to these parameter values Classification tree method can predict state of patient health within bounds starting from 66% to 100%.

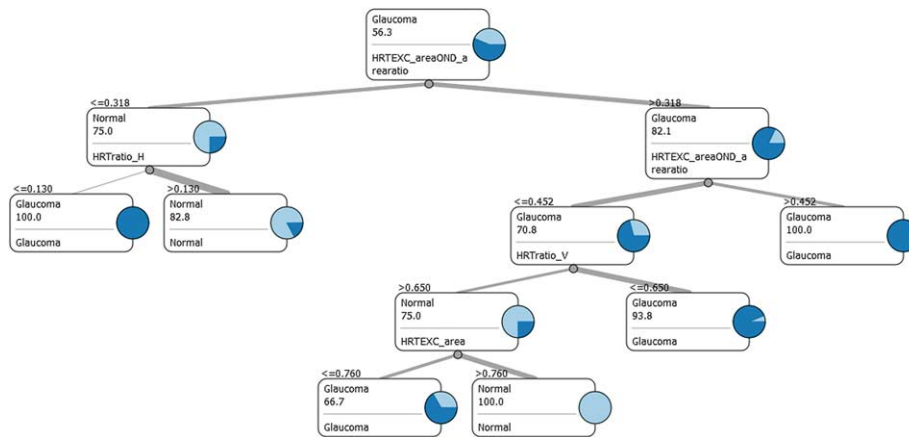


Fig. 3. Classification tree, based on optic nerve disc and excavation parameters, from the Heidelberg Retina tomograph.

When comparing the classification accuracy of both the stereometric and planimetric eye fundus structure parameters estimation the best result is achieved when used parameter set found by HRT, second according to the classification accuracy is when used interactive algorithm parameter set, the third classification accuracy is produced by the automated algorithm parameter set, and the poorest is optical coherence tomography parameter set produced for glaucoma detection.

6. Conclusions

In this paper, the authors have presented a new algorithm for excavation detection and approximation by an elliptic curve. The presented algorithm uses the Bayes optimization algorithm for parameter estimation. The achieved results were compared to those obtained by an interactive algorithm where an ophthalmologist has described the optic nerve disc and excavation interactively by marking the boundary of the excavation and the optic nerve disc with the mouse on the screen. Next, the parameters of the same investigative persons of such advanced techniques as Optical Coherence Tomography and Heidelberg Retina Tomography were compared as well. Finally, the parameters were fetched to classifiers to grasp whether the explicit classification of norm-glaucoma can be made subject to those parameters.

We have concluded that the automated algorithm made 9 mistakes in optical disc parameterization and produced 16 incorrect measurements of the excavation out of 72 images, respectively. The mistakes were made because of the weak anatomical structures pixel intensity gradient change in eye fundus images.

The parameter correlation analysis proves that the automated algorithm recognizes and parameterizes eye fundus structures in a similar manner as an ophthalmologist does. The computed correlation between interactive and automated algorithm excavation pa-

parameter is found to be strong. In a similar manner, the results show that the new technological achievements and different algorithm realization that are capable to perform a laser scan of a human eye fundus and to calculate the optic nerve disc and excavation parameters also produces the strong parameter correlation result. For both planar and stereometric techniques correlation is strong and reaches 0.8.

In addition, the norm-glaucoma classification accuracy was inspected. The classification accuracy is better when the parameters gathered from the interactive algorithm were used. Confusion matrices confirm that a correct class assignment is better with the parameters produced by the interactive algorithm for the norm case (21 patients of 32). However, the glaucoma class identification remains the same with the parameters produced by both methods (26 out of 40). When the parameters of the neuroretinal rim were excluded, the classifier accuracy was better when the parameters, found by the interactive algorithm, were used for the classification. Furthermore, the parameters, obtained by an automated algorithm, suit better for glaucoma detection, since 30 correct glaucoma cases were identified from 40, while the parameter set from the interactive algorithm were able to describe 28 glaucoma cases out of the same 40. Heidelberg Retina Tomography better describe the glaucoma as compared to Optical Coherence Tomography, 30 cases and 21 true positive out of 40 cases, respectively. However, the accomplished investigation reveals that the parameter sets produced by different techniques does not able to describe the glaucoma disease.

When comparing classification accuracy by the different parameter sets the performance queue may be formed. According to the norm-glaucoma classification accuracy the best is Heidelberg Retina tomography technique, the second is interactive algorithm, the third is automated algorithm, and the fourth is Optical Coherence tomography technique for the eye fundus structure parameter estimation.

References

- Bernataviciene, J. (2008). *Methodology of Visual Knowledge Discovery and its Investigation*. Technika, Vilnius.
- Bock, R., Meier, J., Nyul, L., Hornegger, J., Michelson, G. (2010). Glaucoma risk index: automated glaucoma detection from color fundus images. *Medical Image Analysis*, 14(3), 471–481.
- Bourne, R., Foster, P., Bunce, C., Peto, T., Hitchings, R., Khaw, P. (2009). The morphology of the optic nerve head in the Singaporean Chinese population (the Tanjong Pagar study). Part 2. Biometric and systemic associations. *British Journal Ophthalmology*, 92(3), 310–314.
- Breiman, L., Friedman, J., Olshen, R., Stone, C. (1984). *Classification and Regression Trees*. Chapman & Hall, New York.
- Chrastek, R., Wolf, M., Donath, K., Niemann, H., Paulus, D., Hothorn, T. (2005). Automated segmentation of the optic nerve head for diagnosis. *Medical Image Analysis*, 9(4), 297–314.
- Corona, E., Mitra, S., Wilson, M., Krile, T., Kwon, Y., Soliz, P. (2002). Digital stereo image analyzer for generating automated 3-D measures of optic disc deformation in glaucoma. *IEEE Transactions on Medical Imaging*, 21(10), 1224–1253.
- Correnti, A., Wollstein, G., Price, L., Schuman, J. (2003). Comparison of optic nerve head assessment with a digital stereoscopic camera (Discam), scanning laser ophthalmoscopy, and stereophotography. *Ophthalmology*, 110(8), 1499–1505.
- Cristiani, N., Shawe-Taylor, J. (2003). Support vector and kernel methods. In: Berthold, M. and Hand D. (Eds.), *Intelligent Data Analysis*, pp. 169–197

- Curk, T., Demšar, J., Xu, Q., Leban, G., Petrovič, U., Bratko, I. *et al.* (2005). Microarray data mining with visual programming. *Bioinformatics*, 21(3), 396–404.
- Demsar, J., Zupan, B., Leban, G. (2004). *Orange: From Experimental Machine Learning to Interactive Data Mining*, White paper, University of Ljubljana, Faculty of Computer and Information Science.
- Dunham, M.H. (2003). *Data Mining Introductory and Advanced Topics*. Pearson Education, Inc. Prentice Hall.
- Guesalaga, A., Irarrazabal, P., Guarini, M., Alvarez, R. (2003). Measurement of the glaucomatous cup using sequentially acquired stereoscopic images. *Measurement*, 34(3), 207–213.
- Harvey, A., Lakshminarayanan, V. (2010). Imaging in the eye introduction. *Journal of Modern Optics*, 57(2), 93.
- Hoffmann, E., Zangwill, L., Crowston, J., Weinreb, R. (2007). Optic disk size and glaucoma. *Survey of Ophthalmology*, 52(1), 32–49.
- Jayasundera, T., Danesh-Meyer, H., Donaldson, M., Gamble, G. (2005). Agreement between stereoscopic photographs, clinical assessment, Heidelberg retina tomograph and digital stereoscopic optic disc camera in estimating vertical cup: disc ratio. *Clinical and Experimental Ophthalmology*, 33(3), 259–263.
- Jegelevičius, D., Buteikienė, D., Barzdžiukas, V., Paunksnis, A. (2008). Parameterization of the optic nerve disk in eye fundus images. In: *IFMBE Proceedings: NBC-14th Nordic-Baltic Conference on Biomedical Engineering and Medical Physics*, Vol.20(8), pp. 528–531.
- John, G. H., Langley, P. (1995). Estimating continuous distributions in Bayesian classifiers. In: *Eleventh Conference on Uncertainty in Artificial Intelligence*, Morgan Kaufmann, San Mateo, pp. 338–345.
- Joshi, G., Sivaswamy, J., Krishnadas, S. (2010). Optic disk and cup segmentation from monocular color retinal images for glaucoma assessment. *IEEE Transactions on Medical Imaging*, 30(6), 1192–1205.
- Kurasova, O. (2009). Visualization of support vectors. In: *International Conference on Applied Stochastic Models and Data Analysis*. Technika, Vilnius, pp. 522–526.
- Lamoureux, E., Lo, K., Ferraro, J., Constantinou, M., Keeffe, J., Muller, A. (2006). The agreement between the heidelberg retina tomograph and a digital nonmydriatic retina camera in assessing area cup-to-disc ratio. *Investigative Ophthalmology & Visual Science*, 47(1), 93–98.
- Liu, B. (2006). *Web Data Mining – Exploring Hyperlinks, Contents and Usage Data*. Springer, Berlin.
- Morgan, J., Sheen, N., North, R., Choong, Y., Ansari, E. (2005). Digital imaging of the optic nerve head: monoscopic and stereoscopic analysis. *British Journal of Ophthalmology*, 89(7), 879–884.
- Nayak, J., Acharya, U., Bhat, P., Shetty, N., Lim, T. (2009). Automated diagnosis of glaucoma using digital fundus images. *Journal of Medical Systems*, 33(5), 337–346.
- Neubauer, A., Krieglstein, T., Chryssafis, C., Thiel, M., Kampik, A. (2006). Comparison of optical coherence tomography and fundus photography for measuring the optic disc size. *Ophthalmic and Physiological Optics*, 26(1), 13–18.
- O’Colmain, U., Anijeet, D., Vosoughi, M., Sinclair, A., Sanders, R. (2011). Glaucoma blind registration in Fife (2000–2009) – a retrospective cohort study. *Ophthalmic & Physiological Optics*, 31(4), 360–366.
- Paunksnis, A., Barzdžiukas, V., Jegelevičius, D., Kurapkiene, S., Dzemyda, G. (2006). The use of information technologies for diagnosis in ophthalmology. *Journal of Telemedicine and Telecare*, 12(1), 37–40.
- Pearce, J. (2009). The Ophthalmoscope: Helmholtz’s Augenspiegel. *European Neurology*, 61(4), 244–249.
- Quinlan, J. R. (1993). *C4.5: Programs for Machine Learning*. Morgan Kaufmann, San Mateo.
- Raudys, Š. (2001). *Statistical and Neural Classifiers. An Integrated Approach to Design*, 1 edn. Springer, London.
- Rosenblatt, F. (1962). *Principles of Neurodynamics; Perceptrons and the Theory of Brain Mechanisms*. Spartan Books, Washington.
- Sampaolesi, R., Sampaolesi, J., Zárate, J. (2009). *The Glaucomas*. Springer, Berlin.
- Sanfilippo, P., Cardini, A., Hewitt, A., Crowston, J., Mackey, D. (2009). Optic discs morphology – rethinking shape. *Progress in Retinal and Eye Research*, 28(4), 227–248.
- Spaeth, G., Lopes, J., Junk, A., Grigorian, A., Henderer, J. (2006). Systems for staging the amount of optic nerve damage in glaucoma: a critical review and new material. *Survey of Ophthalmology*, 51(4), 293–315.
- The MathWorks Inc. (2007). MATLAB version 7.14.0. The MathWorks Inc., Natick.
- Tiešis, V., Treigys, P. (2010). Optic nerve disc mathematical parameterization and the statistical comparison with measurements. *Lietuvos matematikos rinkinys. Lietuvos matematikų draugijos darbai*, 51, 325–329.
- Treigys, P., Šaltenis, V., Dzemyda, G., Barzdžiukas, V., Paunksnis, A. (2008). Automated optic nerve disc parameterization. *Informatika*, 19(3), 403–420.
- Williams, Z., Pedut-Kloizman, T., Schuman, J. (2011). Disc Analysis. In: *Free Medical Textbook*, pp. 1459–1464.

- Witten, I.H., Frank, E. (2005). *Data Mining: Practical Machine Learning Tools and Techniques*. Morgan Kaufmann.
- Xu, J., Ishikawa, H., Wollstein, G., Bilonick, R., Sung, K., Kagemann, L. (2008). Automated assessment of the optic nerve head on stereo disc photographs. *Investigative Ophthalmology & Visual Science*, 49(6), 2512–2517.

D. Buteikienė 1998 graduated from the Kaunas Medical Academy, in 2003 finished her residency in Ophthalmology at Eye Department, Kaunas University of Medicine, since 2007 is an ophthalmologist in Eye Clinic, Hospital of Lithuanian University of Health Sciences Kaunas Clinics, since 2006 is a junior scientific worker, Department of Ophthalmology, Institute of Neurosciences, Lithuanian University of Health Sciences. In 2007–2011 doctoral studies at Department of Ophthalmology, Institute of Neurosciences, Lithuanian University of Health Sciences. Her present research areas include glaucoma and medical retina, eye fundus image analysis, and laser methods for eye fundus examination.

A. Paunksnis graduated from the Kaunas University of Medicine, Lithuania. Medical doctor since June, 1969. DrSci (habil.) since 1993, professor of ophthalmology since 1997. He is director of the Department of Ophthalmology, Institute for Biomedical Research of Kaunas University of Medicine since July, 1992. Member of the Council of European Ophthalmologist Society since 1995, a full member of the International Society of Experimental Eye Research since 1989, president of the Lithuanian Ophthalmologist Society 1993 to 1997, chairman of the Council of Kaunas University of Medicine 1997 to 2000, coordinator of the Telemedicine Project Group of Kaunas University of Medicine since June 1999, head of the Telemedicine Center of Kaunas University of Medicine since 2002. His present research areas include non-invasive ultrasound examination in ophthalmology, ophthalmooncology, epidemiology, telemedicine.

V. Barzdžiukas 1976 graduated from Kaunas University of Medicine, Lithuania. On 1977 completed internship in ophthalmology in Kaunas Eye Clinic. 1977–1988 – researcher in Sight Protection Laboratory, KMU. Since 1988 DrSci (PhD), 1988 – assistant professor, 1998 – associate professor in Kaunas Eye Clinic. Since 2009 – head of Department of Ophthalmology in Institute of Neurosciences of Lithuanian University of Health Sciences, from 2010 head of Sector of General Ophthalmology, Kaunas Eye Clinic. Present research areas are non-invasive examination of eye circulation, epidemiology, neuroophthalmology, telemedicine, eye image processing.

J. Bernatavičienė graduated from the Vilnius Pedagogical University in 2004 and received a master degree in informatics. In 2008, she received a doctoral degree in computer science (PhD) from Vilnius Gediminas Technical University. She is a researcher at the System Analysis Department of Vilnius University, Institute of Mathematics and Informatics and a lecturer at the Lithuanian University of Educational Sciences. Her research interests include data bases, data mining, visualization, and internet technologies.

V. Marcinkevičius in 2010 received a doctoral degree in computer science (PhD) from Vytautas Magnus University. Since 2001 he is an employee of the Institute of Mathematics and Informatics. His present employment is at the System Analysis Department of the Vilnius University, Institute of Mathematics and Informatics as a researcher. His research interests include data mining in databases, multiple criteria decision support, neural networks, visualization of multidimensional data, and parallel optimization. He is the author of more than 16 scientific publications. He is a member of the Computer Society and Lithuanian Mathematical Society.

P. Treigys graduated from the Vilnius Gediminas Technical University, Lithuania, in 2005. In 2010 received the doctoral degree (PhD) in technical sciences at the Institute of Mathematics and Informatics. He is a member of the Lithuanian Society for biomedical engineering. His interests include: image analysis, detection and object's feature extraction in image processing, automated image objects segmentation, optimization methods, artificial neural networks, and software engineering. Since 2005 he takes lectureship at the Vilnius Kolegija/University of Applied Sciences.

Interaktyvių ir automatinių regos nervo disko ir ekskavacijos parametrizavimo metodų vertinimas

Dovilė BUTEIKIENĖ, Alvydas PAUNKSNIS, Valerijus BARZDŽIUKAS,
Jolita BERNATAVIČIENĖ, Virginijus MARCINKEVIČIUS, Povilas TREIGYS

Glaukoma yra viena iš klastingiausių akių ligų, kurios atsiradimo ir progresavimo žmogus nejaučia. Šiame straipsnyje trumpai apžvelgiami akies nervo disko parametrizavimo būdai ir algoritmai. Parametrizavimas leidžia vienareikšmiškai nusakyti akies nervo disko struktūrą, ir vėliau naudoti tiriant ligų atpažinimo uždavinius ar atliekant kitus tyrimus, kuriems reikalinga parametrinė akies dugne esančių struktūrų išraiška. Iki šiol planimetrinis visiškai automatinis ekskavacijos parametrizavimo uždavinys mokslinėje literatūroje nebuvo išsamiai nagrinėtas. Šiame straipsnyje autoriai aprašo automatinę ekskavacijos parametrizavimo algoritmą bei atlieka tiek automatinio būdu, tiek interaktyviu būdu gautų parametrų koreliacijų analizę. Pristatomi rezultatai yra lyginami su optinės koherentinės ir Heidelbergo tomografijos metu gautais akies dugno struktūrų parametriniais įverčiais. Taip pat straipsnyje aptariamas sveikas-glaukoma klasifikavimo rezultatas atsižvelgiant į minėtų technologijų pagalba gautus akies dugno anatomiinių struktūrų parametrus.